Inorganic Chemistry

Article

pubs.acs.org/IC

Spin-Reorientation Transition in CeMnAsO

Alex J. Corkett, David G. Free, and Simon J. Clarke*

Inorganic Chemistry Laboratory, Department of Chemistry, University of Oxford, South Parks Road, Oxford OX1 3QR, U.K.

Supporting Information

ABSTRACT: High-resolution X-ray and neutron powder diffraction are used to reveal details of the spin-reorientation transition in the layered oxide pnictide CeMnAsO. Above 38 K, the localized moments on Mn^{2+} are antiferromagnetically ordered in a checkerboard fashion within the antifluorite-type MnAs planes and are oriented perpendicular to the planes. Below 38 K, reorientation of these moments into the planes commences. This is complete by 34 K and is coincident with long-range ordering of the Ce^{3+} moments. The Ce^{3+} and Mn^{2+} moments have an arrangement that is different in detail from that in the isostructural NdMnAsO and PrMnSbO. There is no evidence for structural distortion, as found for PrMnSbO and related Pr^{3+}-containing compounds, although there is evidence for a very slight (0.025%) misfit between the magnetic and structural cells below the spin-reorientation transition. It is clarified that neutron powder diffraction methods are unable to distinguish between collinear and noncollinear arrangements of manganese and lanthanide moments when the moments have a component parallel to the MnAs planes. A proposal from computational analysis that NdMnAsO and CeMnAsO should adopt different magnetic structures on the basis of the different balances between biquadratic and antisymmetric exchange interactions should be tested using alternative methods.

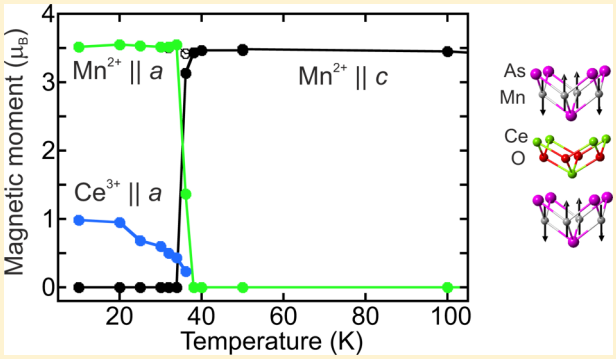

INTRODUCTION

Compounds with the common ZrCuSiAs-type structure (Figure 1;[1,2] sometimes described as the $HfCuSi_2$-type

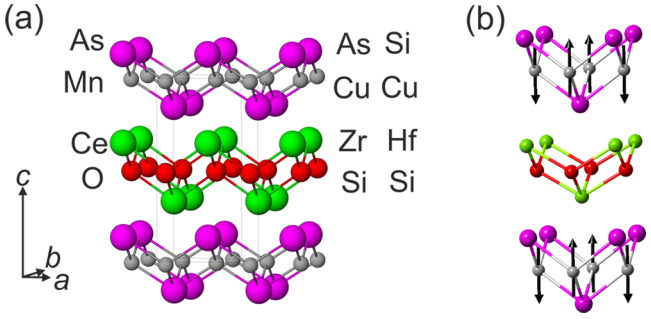

Figure 1. (a) Diagram of the CeMnAsO structure with an alternative labeling showing the arrangement of atoms in ZrCuSiAs and $HfCuSi_2$, which are the compounds commonly used to describe the structure type. (b) Model for magnetic ordering on the Mn^{2+} sublattice only in LnMnPnO (Pn = pnictide) systems.

structure) show diverse electronic, magnetic, and structural properties. The diversity of compositions is illustrated by members of the iron-based superconductors, which include many compounds with this so-called (to reflect the stoichiometry) "1111" structure containing FeAs antifluorite-type layers, notably $LaFeAsO_{1-x}F_x$,[3] SrFeAsF,[4,5] and $(Ca_{1-x}La_x)FeAsH$[6] and derivatives. These compounds of iron alone reveal extremely rich phase diagrams in which the physical properties depend on the composition or an applied hydrostatic pressure and in which there is strong competition between itinerant antiferromagnetic (AFM) long-range order and unconventional superconductivity.[7−9]

Substitution on all of the crystallographic sites of the structure is possible. For oxide pnictides, with lanthanide ions coordinating to oxide to form fluorite-type LnO layers and formally divalent ions of middle-to-late transition metals coordinated by the pnictogens (P, As, and Sb) in antifluorite-type MPn layers, the electronic classification of the compounds depends mainly on the identity of the transition-metal ion. The Mn^{2+} series of LnMnAsO (Ln = Y, La, Ce, Pr, Nd, Sm, Gd, Tb, Dy, U) compounds, with MnAs antifluorite layers, was first synthesized by Nientiedt et al. in 1997.[10] These are Mott−Hubbard insulators with large localized moments on Mn^{2+}. The Fe^{2+} analogues are semimetallic itinerant antiferromagnets lying in close proximity to an unconventional superconducting state.[3,11] The Co^{2+}-containing compounds LnCoAsO (Ln = La, Ce, Pr, Nd, Sm, Gd) are metallic itinerant ferromagnets with small ordered moments associated with Co^{2+} below 70−100 K. When the lanthanide ion carries a magnetic moment, lower temperature magnetic transitions are evident associated with magnetic ordering of the lanthanide moment and its interaction with the cobalt moment, and these lead to AFM ground

Special Issue: To Honor the Memory of Prof. John D. Corbett

Received: November 4, 2014
Published: December 3, 2014

   dx.doi.org/10.1021/ic5026608 | Inorg. Chem. 2015, 54, 1178−1184

states.[12−14] Nickel analogues exhibit what appears to be conventional phonon-mediated superconductivity with T_c < 4 K and show electronic properties quite different from the iron analogues, which are unconventional high-T_c superconductors.[15] The two extra d electrons supplied by Ni^{2+} (d^8) compared to Fe^{2+} (d^6) raise the Fermi level to generate a Fermi surface that is quite unlike that of the FePn-based superconductors.[16]

In the wake of the interest in iron-based superconductors, the physical properties of these compounds and relatives with similar structural motifs have received fresh attention. The manganese compounds containing Mn^{2+} ions contrast with the iron, cobalt, and nickel analogues in that the Mn^{2+} ions carry large localized moments that undergo AFM ordering above ambient temperatures. In the absence of magnetic ordering of the moments carried by other magnetic ions in the compounds, the manganese moments within the MnE antifluorite-type layers (E = Si, Ge, P, As, Sb, Bi) order in a "checkerboard-type" arrangement, with nearest-neighbor moments coupled antiferromagnetically and the moments oriented perpendicular to the layers as in a single MnPn layer of the LnMn*Pn*O systems shown in Figure 1b. For example, $BaMn_2As_2$ with the $ThCr_2Si_2$ structure[17] exhibits AFM ordering of Mn^{2+} moments below T_N = 625 K [saturated ordered moment of 3.88(4) μ_B at 10 K]. In this case, it is found that the nearest-neighbor manganese moments in adjacent layers are aligned antiferromagnetically, so overall a G-type magnetic structure is adopted. Such an arrangement is found in many related Mn^{II} compounds including the pnictides KMnAs,[18] RbMnSb, CsMnAs, and CsMnSb[19] and the tetrelides SrMnGe, SrMnSn, and BaMnGe[20] with the PbFCl/Cu_2Sb structure type, $SrMnBi_2$[21] with the $HfCuSi_2$ structure type (MnBi layers are separated by SrBi layers), and the oxide pnictides $Sr_2MnO_2Mn_2Pn_2$ (Pn = As, Sb),[22] where MnPn antifluorite layers are separated by Sr_2MnO_2 oxide layers. In contrast, in the LnMnAsO compounds with Ln = La or Nd,[23,24] NaMnPn (Pn = P, As, Sb, Bi),[18] the tetrelides MgMnGe, CaMnSi, CaMnGe, and CaMnSn,[20] and other cases such as $CaMnBi_2$,[21] there is ferromagnetic (FM) alignment of the nearest-neighbor moments in adjacent layers, so overall a C-type magnetic structure is adopted. There is presumably a small energy difference between the alignment being AFM or FM along the direction perpendicular to the layers. LnMnGe (Ln = La, Ce, Pr),[25] which are formally Mn^{I} compounds, also display this magnetic ordering.

In the LnMnPnO compounds, the magnetic ordering of the Mn^{2+} sublattice is influenced by lanthanide magnetism at low temperatures. On cooling below 23 K, NdMnAsO undergoes a well-characterized spin reorientation of the manganese moments.[23,24] At high temperatures, the magnetic structure is like that shown in Figure 1b, but at low temperature, the moments lie in the *ab* plane. This reorientation of the Mn^{2+} moment direction is accompanied by long-range AFM ordering of the Nd^{3+} moments, which also lie within the *ab* plane, and occurs without a change in the magnetic propagation vector nor with any measurable symmetry-lowering structural distortion. In contrast, LaMnAsO, with no 4f electrons, exhibits no such spin-reorientation transition and retains the structure in Figure 1b at all temperatures. As has been discussed elsewhere,[26] the temperature at which the lanthanide moments exhibit magnetic long-range order is much higher than one would expect were these the only magnetic ions in the compound. The picture in NdMnAsO is that the interaction between the Nd^{3+} and Mn^{2+} moments drives the ordering of the Nd^{3+} moment and the reorientation of the Mn^{2+} spin direction. In the Pr^{3+} analogue PrMnSbO (with Sb replacing As),[27] there is a similar spin-reorientation transition at around 80 K; furthermore, at 35 K there is a symmetry-lowering transition from *P*4/*nmm* to *Pmmn* symmetry, which may be resolved using high-resolution diffractometers, and at 4 K the two basal lattice parameters differ by 0.018 Å (0.43%). This distortion is ascribed to a cooperative local distortion of the $4f^2$ Pr^{3+} ion.[27] We note here that for tetragonal systems neutron powder diffraction (NPD) is fundamentally unable to determine the direction of the Mn^{2+} and lanthanide moments within the *ab* plane, as described by Shirane,[28] and even whether the manganese and lanthanide moments are collinear or not, as noted explicitly by Marcinkova et al. in ref 23. The magnetic structure depicted in refs 23 and 24 is a possible model that accounts for the observed scattering of NdMnAsO. We show in Figure 2 possible magnetic models grouped into cases A−C according to their NPD patterns, and we return to this point in the Results and Discussion.

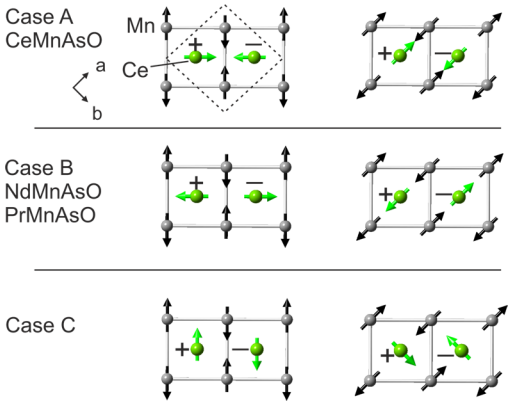

Figure 2. Possible magnetic structures with propagation vectors k = (0, 0, 0) for LnMnPnO compounds when the Mn^{2+} and lanthanide moments are both ordered and the moments lie in the *ab* plane. For tetragonal crystal structures, cases A−C are distinguishable from one another in NPD experiments, but it is not possible to distinguish the collinear (i.e., all moments parallel or antiparallel) and noncollinear models shown for each case because of the perfect overlap of reflections. The models in case B produce the scattering observed in both NdMnAsO[23,24] and PrMnSbO.[27] We note that the diagrams in ref 29, which makes computational predictions of the ordering in NdMnAsO and CeMnAsO, distinguish the three cases and designate the noncollinear models of cases A and B as ||*ab*-O1 and ||*ab*-O2, respectively, and the collinear model of case C as ||*ab*-C. Further discussion is provided in the text, and the differences in the magnetic scattering of the three cases are shown in the Supporting Information (SI). The + and − symbols indicate lanthanide ions above or below the manganese plane, respectively. The unit cell is indicated by the dotted line.

While we focus on manganese compounds in this paper, we note that a different magnetic ordering transition controlled by the lanthanide ion is observed in the cobalt analogue NdCoAsO in which the relative spin orientation between the planes changes.[13] Similar control of the magnetic ordering has been described in the germanide and silicide analogues; i.e., magnetic lanthanide ions induce a spin-reorientation transition of the manganese moments as the lanthanide moments order, and the Pr^{3+} compounds PrMnSi and PrMnGe exhibit a symmetry-lowering distortion.[25]

dx.doi.org/10.1021/ic5026608 | *Inorg. Chem.* 2015, 54, 1178−1184

A recent investigation of some of the physical properties of CeMnAsO by Tsukamoto et al.[26] reveals a transition in the heat capacity that suggests that a spin reorientation also takes place, and the nature of the transition indicates that, like in NdMnAsO, it occurs without the crystallographic distortion found in PrMnSbO.[27] A computational investigation,[29] furthermore, suggests that the reorientation transitions in CeMnAsO and NdMnAsO should be different. The arrangement of the magnetic cations results in zero net Heisenberg exchange between the ordered Mn^{2+} sublattice and the Ln^{3+} sublattice, so the interaction is dominated by biquadratic (BQ) and/or antisymmetric (DM) exchange (Dzalozhinskii−Moriya exchange) terms. The prediction is that for NdMnAsO the BQ exchange between Mn^{2+} and Nd^{3+} dominates the DM exchange term by about 18 meV/formula unit and results in a collinear arrangement of Mn^{2+} and Nd^{3+} spins. We note here that in ref 29 this arrangement of spins is depicted as the collinear model of case C in Figure 2, with the Mn^{2+} moments directed along the Mn−Mn bonds, which would not account for the scattering observed experimentally in NdMnAsO, which corresponds to the case B models.[23,24] In contrast, the computational prediction[29] for CeMnAsO is that the DM exchange term dominates the BQ exchange term by about 5 meV/formula unit, and the magnetic structure that results is one in which Mn^{2+} and Ce^{3+} moments are confined within parallel planes but oriented orthogonal to one another below the spin-reorientation transition. As we describe in more detail in the Results and Discussion, none of these predictions can be confirmed by NPD experiments on tetragonal systems.

EXPERIMENTAL SECTION

Synthesis. CeMnAsO samples were prepared on the 1−3 g scale by the solid-state reaction between CeAs [prepared by the reaction of freshly filed cerium (Alfa 99.8%) and crushed arsenic lumps (Alfa 99.999%) at 800 °C], CeO_2 (Alfa 99.99%), and further arsenic and manganese powder (Alfa 99.95%) in a 1:1:1:2 ratio. The mixture was homogenized using an agate pestle and mortar, pressed into a pellet at a force of 5 tonnes, placed in an alumina crucible, and then sealed in a silica ampule under a dynamic vacuum. The sample was then heated at a rate of 1 °C/min to 1100 °C (the slow heating rate ensures that the volatile arsenic reacts before it can develop a high vapor pressure) and held at this temperature for 48 h. The resultant black crystalline powder was stored in an argon drybox.

Structural Characterization. Ambient- and low-temperature powder X-ray diffraction (PXRD) data were collected on portions of 1 and 3 g samples on beamline ID31 at ESRF, Grenoble, France, using 0.35 and 0.4 Å X-rays, respectively, and with the samples contained in 0.5-mm-diameter borosilicate capillaries. Rietveld analysis of the data was performed using the *TOPAS-Academic* software.[30] NPD data were collected on the 3 g sample using the OSIRIS diffractometer, optimized for high resolution at relatively long *d* spacings, and the higher-resolution powder diffractometer (HRPD), optimized for high resolution at short *d* spacings, both at the ISIS Facility, U.K. Rietveld refinements incorporating magnetic phases were performed using the *GSAS* suite[31] via the *EXPGUI* interface,[32] and the *SARAh* representational analysis program[33] was interfaced with *GSAS* to enable a full investigation of the magnetic ordering. On OSIRIS and HRPD, the 3 g sample was contained in a thin-walled vanadium cylinder, and all measurements were performed inside an aluminum-tailed (OSIRIS) or vanadium-tailed (HRPD) cryostat. On OSIRIS, Bragg reflections from the walls of the aluminum cryostat were well modeled using the model-independent Le Bail method as arising from two aluminum phases with different lattice parameters to account for their displacement from the diffractometer axis.

Magnetometry. Magnetometry data were collected using a Quantum Design MPMS5-XL SQUID magnetometer. Samples of about 30 mg in mass were contained in gelatin capsules.

RESULTS AND DISCUSSION

Magnetometry. The magnetic susceptibility of CeMnAsO (Figure 3) was determined from the difference between

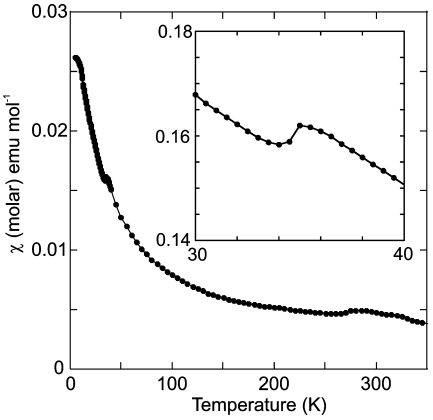

Figure 3. Temperature dependence of the magnetic susceptibility between 350 and 2 K. The inset shows the transition that is investigated below by diffraction methods. The broad feature between 270 and 330 K arises from subtraction of the contribution of the FM impurity MnAs (T_c = 318 K; see Figure S1 in the SI).

temperature-dependent measurements in applied fields of 4 and 3 T, a region of applied fields in which the magnetization of a small MnAs FM impurity was saturated and the sample magnetization was thus found to vary linearly with the applied field (see Figure S1 in the SI). An abrupt maximum is observed in the susceptibility at 35 K. This was also observed by Tsukumoto et al.,[26] who ascribed it to a spin reorientation of Mn^{2+} moments concomitant with the onset of Ce^{3+} ordering based on the observation of a similar phenomenon in NdMnAsO.[23,24] The magnetic properties of the samples prepared by us using stoichiometric mixtures at 1100 °C compare well with those of samples prepared using a different synthetic route (2:1 ratio of CeAs and Mn_2O_3 heated at 1000 °C in the presence of a titanium oxygen getter) by Tsukumoto et al.[26]

Crystal and Magnetic Structures. *Ambient Temperature.* Rietveld refinement against ambient temperature ID31 data are shown in Figures 4 and S2 in the SI. Refined structural parameters are given in Table 1.

The 1 g sample was found to contain about 1 mol % CeO_2, and the 3 g sample measured using NPD contained 2.88(5) mol % CeO_2 and 3.36(6) mol % MnAs (Figure S2 in the SI). The additional phases were included in the refinement together with the main CeMnAsO nuclear phase and aluminum reflections from the cryostat ($Fm\bar{3}m$; $a \approx 4.03$ Å). Because MnAs orders ferromagnetically above room temperature (T_C = 318 K), a single Le Bail (model-independent) phase was used to model both the nuclear and magnetic contributions to the Bragg reflections from this phase. A broad peak between 2.25 and 2.31 Å was also observed, could not be indexed, but was also observed in data collected on structurally unrelated materials in the same experimental period, and so was deemed to be instrumental in origin, and this region was excluded from the refinement. Additional Bragg intensity was evident in the

dx.doi.org/10.1021/ic5026608 | *Inorg. Chem.* 2015, 54, 1178−1184

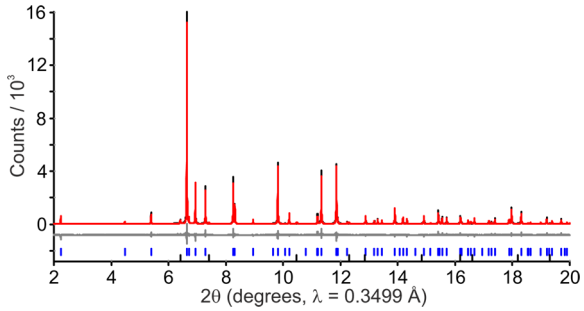

Figure 4. Rietveld fit to synchrotron PXRD data (ID31) for a 1 g sample of CeOMnAs collected at 295 K. The data, fit, and difference curves are shown, and tick marks show the reflection positions for CeMnAsO (upper blue markers) and a 1 mol % CeO_2 impurity phase (lower black markers). CeMnAsO: *P*4/*nmm*, a = 4.09081(2) Å, c = 8.96789(6) Å, V = 150.075(2) Å^3; R_{wp} = 14.75, χ^2 = 1.89. See Table 1 and Figure S2 in the SI.

Table 1. Fractional Coordinates and Site Occupancies for CeMnAsO from ID31 Data[a]

atom	site	x	y	z	occ.	$100U_{iso}$/Å^2
Ce	2c	0.25	0.25	0.13174(7)	1	0.98(2)
O	2a	0.75	0.25	0	1	1.7(2)
Mn	2b	0.75	0.25	0.5	1	0.40(5)
As	2c	0.25	0.25	0.67005(12)	1	0.80(4)

[a]Space group *P*4/*nmm* (No. 129) (setting number 2 chosen: inversion center at the origin).

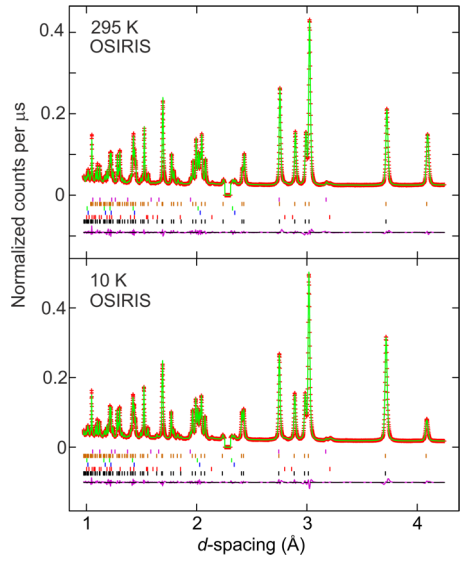

Figure 5. Rietveld fits against OSIRIS data at ambient temperature and 10 K. The plots show the data (red), fit (green), difference (purple), and the reflection positions are marked (from bottom to top) for the phases: CeMnAsO (nuclear; black markers); MnAs (nuclear; red markers); two aluminum phases from the sample environment (blue and green markers); CeMnAsO (magnetic; brown markers); CeO_2 (nuclear; purple markers). The magnetic model at 295 K is that depicted in Figure 1b and that at 10 K is accounted for by the models in case A in Figure 2. See also Table S1 in the SI.

room temperature data, which could not be accounted for by the nuclear CeMnAsO phase or impurity phases (Figure S3 in the SI). All of these extra reflections could be indexed on a cell with the same dimensions as those of the CeMnAsO nuclear phase and were assigned to a magnetic unit cell with a propagation vector **k** = (0, 0, 0). We assumed that at room temperature only the manganese moments would contribute to the magnetic Bragg scattering. The SARAh representational analysis and SARAh refine programs[33] were used to determine the magnetic structures. This analysis showed that the only model compatible with the room temperature data was one in which nearest-neighbor manganese moments are arranged antiferromagnetically, ordered manganese moments are aligned along the c axis, and manganese moments related by the lattice vector **c** are aligned parallel (Figure 1b), as in a wide range of related compounds described in the Introduction. There was no evidence for any canting of the moments at room temperature. The Rietveld fit to room temperature PND data including the CeMnAsO magnetic phase is shown in Figure 5, and important structural parameters and global fitting parameters are detailed in Table S1 in the SI. The refined manganese moment at 295 K of 2.65(1) μ_B is similar to those reported by Emery et al.[24] in isostructural LaMnAsO [2.43(1) μ_B] and NdMnAsO [2.35(2) μ_B] materials. The latter has T_N = 359 K, suggesting that CeMnAsO has a similar Neél temperature for the manganese moments, which is outside the measuring range of our instrument. On cooling to 100 K, the moment of 3.46(1) μ_B is close to its saturation value and significantly lower than that expected for free ion Mn^{2+} (5 μ_B). The reduction in the size of the ordered moment because of covalency in the Mn−Pn bonding and direct Mn−Mn interactions across shared tetrahedral edges is comparable to that found in related compounds.[22]

A comparison of the PND patterns collected at 295 and 10 K (Figure 5) shows a considerable difference in the relative intensities of reflections with magnetic contributions (see also Figure S3 in the SI). NPD measurements showed that the changes in the relative intensities occurred on cooling from 38 to 34 K. This coincides with the abrupt maximum observed in the susceptibility at 35 K, which given that the susceptibility is dominated by cerium at this temperature, because the ordering of the manganese moments has saturated, indicates AFM ordering of cerium moments. No additional reflections are observed, implying that a propagation vector of **k** = (0, 0, 0) is retained. A small magnetic contribution to the (0, 0, 2) reflection becomes evident at low temperatures. This and the very large changes in the relative intensities of the other magnetic reflections were suggestive of a spin reorientation of the Mn^{2+} moments as proposed by Tsukamoto et al.[26] and well documented in several related compounds with magnetic lanthanide ions between the MnAs (or MnSi and MnGe) sheets[23−25,27] rather than simple additional ordering of the Ce^{3+} moments.

SARAh representational analysis was undertaken on data collected at 10 K in the space group *P*4/*nmm*, with a **k** = (0, 0, 0) propagation vector and with Ce^{3+} included along with Mn^{2+} as a magnetic atom. This analysis ruled out FM arrangements of manganese and cerium moments and AFM arrangements with moments oriented along the z axis, which did not model the observed magnetic data at low temperatures, indicating that a spin-reorientation transition had occurred. Subsequent analysis showed that models with a collinear arrangement of Mn^{2+} and Ce^{3+} moments with the moments directed along a basal crystallographic axis or an orthogonal arrangement of Mn^{2+} and Ce^{3+} moments with the Mn moments directed parallel to the Mn−Mn direction (i.e., the a + b direction) accounted equally well for the magnetic scattering from a powder. These are the

dx.doi.org/10.1021/ic5026608 | Inorg. Chem. 2015, 54, 1178−1184

models depicted as case A in Figure 2 (see also Figure S4 in the SI). Refined ordered moments of 3.574(9) μ_B for manganese and 1.01(1) μ_B (which seems, from the temperature dependence, to be close to the saturation value) for cerium were obtained at 10 K. The Rietveld fit using this model is shown in Figure 5. In the temperature range of the spin-reorientation transition, the magnetic Bragg intensity was well modeled by manganese moments with contributions from both m_x and m_z.

It seems likely, as in the case of NdMnAsO, that the spin reorientation of the spin-only manganese moments originates from the single-ion anisotropy of the rare-earth moment. Above the spin-reorientation transition, only the Mn^{2+} ($S = {}^5/_2$ and $L = 0$) moments are ordered, and these are directed along the c axis. The Ce^{3+} and Mn^{2+} moments are evidently not independent. The relatively high ordering temperature for the cerium sublattice suggests that the cerium order is driven by interaction with the already ordered Mn^{2+} moments. The single-ion anisotropy of Ce^{3+} ($S = {}^1/_2$ and $L = 3$) dictates that the ordered Ce^{3+} moments lie in the basal plane and the relatively isotropic manganese moment follows the cerium moment, leading to the observed spin reorientation.

While NPD data are not able to distinguish the collinear and noncollinear models for the tetragonal CeMnAsO and NdMnAsO systems, the differences in the relative intensities of the (0, 1, 0)/(1, 0, 0) and (1, 0, 1)/(0, 1, 1) reflections between CeMnAsO and NdMnAsO (see Figure S4 in the SI) do allow us to say that the details of the magnetic ordering in the two cases are different. CeMnAsO corresponds to case A in Figure 2, while NdMnAsO corresponds to case B. The origin of this is not clear. The prediction that the balance of the BQ and DM exchange terms is different in the two compounds[29] might account for the difference. We should note here some confusion relating to the different magnetic models. The collinear model depicted in Figure 3b of ref 29 does not actually account for the magnetic scattering in either NdMnAsO or CeMnAsO. It is a collinear model with the moment directions parallel to the Mn−Mn bonds, which corresponds to case C in Figure 1, and this can be distinguished in a NPD experiment from cases A (CeMnAsO) and B (NdMnAsO) (see Figure S4 in the SI). So, it is not certain that the predicted[29] collinear arrangement of the spins is actually observed in NdMnAsO, and correspondingly we cannot determine from our experiments whether CeMnAsO differs from NdMnAsO in the relative orientations of the manganese and lanthanide spins. We further make the observation that, from the relative intensities of the magnetic Bragg reflections, PrMnSbO adopts a magnetic structure corresponding to case B of Figure 2, like NdMnAsO. However, ref 27 depicts the collinear model of case A, which would give a distribution of Bragg intensities different from that observed. In principle, the structural distortion in PrMnSbO, which lowers the symmetry to orthorhombic, allows collinear and noncollinear models to be distinguished, and it is stated in ref 27 that this would permit the orientation within the planes to be resolved in that case.

Refinements against the OSIRIS NPD data for CeMnAsO with the magnetic and nuclear phases constrained to have the same lattice parameters showed a sharp increase in the refined value of the basal lattice parameters by 0.025% on cooling through the transition. This anomaly was much larger than the estimated standard deviations on the lattice parameters obtained in an individual Rietveld refinement and coincided with the rapid changes in the relative intensities of the magnetic reflections during spin reorientation. Figure 6b shows that in

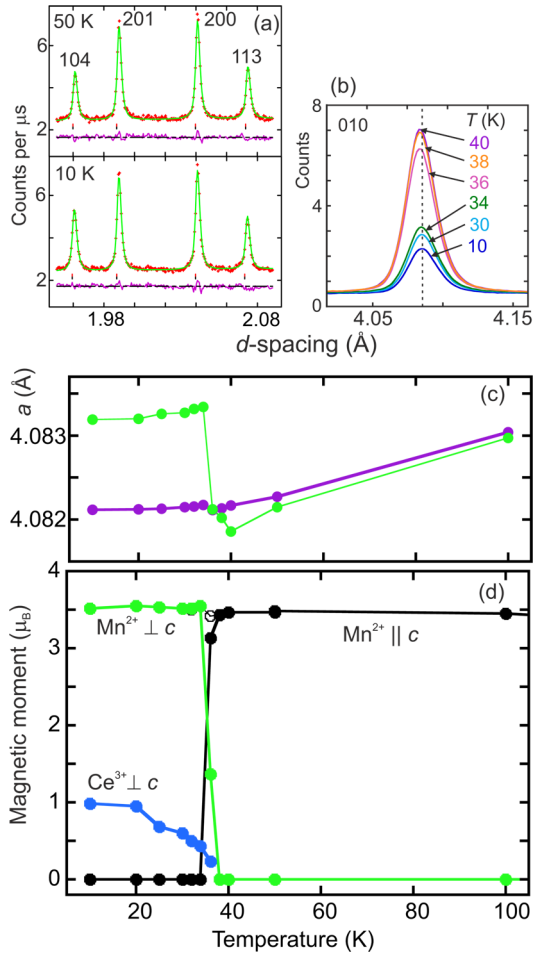

Figure 6. (a) Portions of refinements against HRPD data above (50 K) and below (10 K) the spin-reorientation transition showing the absence of any orthorhombic distortion of the nuclear structure. (b) Shift to higher d spacing on cooling, measured on OSIRIS, of the (0, 1, 0) reflection, which is purely magnetic in origin and changes its intensity markedly through the transition. (c) Corresponding increase in the refined a lattice parameter for the magnetic cell through the transition compared with the smooth behavior of the corresponding parameter for the nuclear cell (from refinements against OSIRIS data in which independent tetragonal cells were refined stably for the nuclear and magnetic structures). (d) Evolution with the temperature of the refined magnetic moments on manganese and cerium ions (the open circle is the total Mn^{2+} moment in the transition region). Error bars corresponding to the estimated standard deviations obtained from GSAS lie within the symbols. The magnetic model used is case A from Figure 2.

the OSIRIS data there is a clear increase in the d spacing of the purely magnetic (1, 0, 0)/(0, 1, 0) reflection on cooling in the region between 36 and 34 K, where the intensity changes dramatically. Note that, because neutrons interact only with the projection of a magnetic moment in the plane perpendicular to the vector of that moment, then the arbitrary choice of alignment of manganese and cerium moments along a (rather than b) in the collinear model of case A means that the magnetic Bragg intensity would only be observed for the (0, 1, 0) reflection and not the (1, 0, 0) reflection. Therefore, a plausible scenario was an orthorhombic distortion in which the d spacings of (0, 1, 0) and the zero intensity of (1, 0, 0) became separate, and this would confirm the collinear magnetic model of case A. This was investigated more closely to examine

dx.doi.org/10.1021/ic5026608 | Inorg. Chem. 2015, 54, 1178−1184

whether there was a small orthorhombic distortion an order of magnitude smaller than that found in PrMnSbO[27] or whether the shift in the *d* spacing had some other origin. Refinements against diffraction data obtained from the ID31 high-resolution X-ray diffractometer at ESRF revealed a smoothly varying basal cell parameter and no discernible symmetry lowering through the spin-reorientation transition (Figure S2b in the SI), even though the resolution is so high that a distortion an order of magnitude smaller than that suggested by the refinements against OSIRIS data would have been observable. Similarly, refinements at 10, 30, and 50 K against data collected by HRPD at ISIS, using the same sample that was measured on OSIRIS and where the resolution below 2.5 Å is extremely high, showed no broadening of the reflections (Figure 6a). We conclude from using extremely high-resolution diffractometers that there is no measurable lowering of the crystallographic symmetry through the spin-reorientation transition.

In the absence of structural distortion, the shift in the position of the magnetic Bragg peaks through the spin-reorientation transition suggests that at the transition the magnetic structure becomes slightly incommensurate with the crystal structure with a modulation vector component of 0.99975 in the *a* (and/or *b*) direction. Given the small (0.025%) deviation of the modulation vector from 1 and the lack of any additional reflections observable above the background in the powder pattern, which might have enabled a more complex magnetic structure to be modeled, the OSIRIS data were analyzed with both the nuclear and magnetic unit cells constrained to be tetragonal, but with decoupled *a* lattice parameters, and the values obtained from these stable refinements are plotted as a function of the temperature in Figure 6c. Figure 6d shows the evolution of the magnitude of the magnetic moments and their direction relative to the unique axis.

CONCLUSIONS

CeMnAsO exhibits magnetic ordering of the Mn^{2+} sublattice from the above ambient temperatures to a spin-reorientation transition at ∼35 K, which coincides with the ordering of the Ce^{3+} sublattice. The magnetic structure of the low-temperature magnetic phase is different in detail from that found for several related compounds, including the isostructural compound NdMnAsO, although the computational prediction[29] that different magnetic structures should be adopted by CeMnAsO and NdMnAsO on account of the different relative sizes of the DM and BQ exchange terms cannot be verified by any of the powder diffraction measurements so far carried out on these compounds. Single-crystal neutron diffraction measurements would, in principle, be able to distinguish the possible models. Our refinements against high-resolution PXRD and NPD data show no evidence for a crystallographic distortion in CeMnAsO, but through the spin-reorientation transition, relative shifts in the positions of the nuclear and magnetic Bragg peaks suggest that a tiny incommensurability develops between the structural and magnetic unit cells, which is only evident using a neutron diffractometer with a high resolution in the long *d*-spacing region.

ASSOCIATED CONTENT

Supporting Information

Magnetization isotherms, additional analysis of high-resolution PXRD data, powder diffractograms expected from different magnetic ordering models, and tables of refined structural parameters. This material is available free of charge via the Internet at http://pubs.acs.org.

AUTHOR INFORMATION

Corresponding Author

*E-mail: simon.clarke@chem.ox.ac.uk.

Notes

The authors declare no competing financial interest.

ACKNOWLEDGMENTS

We thank Dr. C. Curfs for assistance on ID31, Dr. F. Demmel for assistance with OSIRIS, and Dr. A. Daoud-Aladine for assistance with HRPD. We acknowledge the financial support of EPSRC (Grant EP/I017844/1 and a studentship to A.J.C.).

REFERENCES

(1) Pöttgen, R.; Johrendt, D. *Z. Naturforsch. B* **2008**, *63*, 1135−1148.
(2) Muir, S.; Subramanian, M. A. *Prog. Solid State Chem.* **2012**, *40*, 41−56.
(3) Kamihara, Y.; Watanabe, T.; Hirano, M.; Hosono, H. *J. Am. Chem. Soc.* **2008**, *130*, 3296−3297.
(4) Matsuishi, S.; Inoue, Y.; Nomura, T.; Yanagi, H.; Hirano, M.; Hosono, H. *J. Am. Chem. Soc.* **2008**, *130*, 14428−14429.
(5) Tegel, M.; Johansson, S.; Weiss, V.; Schellenberg, I.; Hermes, W.; Pöttgen, R.; Johrendt, D. *Europhys. Lett.* **2008**, *84*, 67007.
(6) Muraba, Y.; Matsuishi, S.; Hosono, H. *J. Phys. Soc. Jpn.* **2014**, *83*, 033705.
(7) Johrendt, D. *J. Mater. Chem.* **2011**, *21*, 13726−13736.
(8) Fujitsu, S.; Matsuishi, S.; Hosono, H. *Int. Mater. Rev.* **2012**, *57*, 311−327.
(9) Hirschfeld, P. J.; Korshunov, M. M.; Mazin, I. I. *Rep. Prog. Phys.* **2011**, *74*, 124508.
(10) Nientiedt, A. T.; Jeitschko, W.; Pollmeier, P. G.; Brylak, M. *Z. Naturforsch.* **1997**, *52b*, 560−564.
(11) de la Cruz, C.; Huang, Q.; Lynn, J. W.; Li, J.; Ratcliff, W.; Zarestky, J. L.; Mook, H. A.; Chen, G. F.; Luo, J. L.; Wang, N. L.; Dai, P. *Nature* **2008**, *453*, 899−902.
(12) Sarkar, R.; Jesche, A.; Krellner, C.; Baenitz, M.; Geibel, C.; Mazumdar, C.; Poddar, A. *Phys. Rev. B* **2010**, *82*, 054423. Yanagi, H.; Kawamura, R.; Kamiya, T.; Kamihara, Y.; Hirano, M.; Nakamura, T.; Osawa, H.; Hosono, H. *Phys. Rev. B* **2008**, *77*, 224431.
(13) McGuire, M. A.; Gout, D. J.; Garlea, V. O.; Sefat, A. S.; Sales, B. C.; Mandrus, D. *Phys. Rev. B* **2010**, *81*, 104405.
(14) Ohta, H.; Yoshimura, K. *Phys. Rev. B* **2009**, *80*, 184409.
(15) Watanabe, T.; Yanagi, H.; Kamihara, Y.; Kamiya, T.; Hirano, M.; Hosono, H. *J. Solid State Chem.* **2008**, *181*, 2117−2120. Subedi, A.; Singh, D. J.; Du, M.-H. *Phys. Rev. B* **2008**, *78*, 060506.
(16) Kurita, N.; Ronning, F.; Miclea, C. F.; Bauer, E. D.; Gofryk, K.; Thompson, J. D.; Movshovich, R. *Phys. Rev. B* **2011**, *83*, 094527. Subedi, A.; Singh, D. J. *Phys. Rev. B* **2008**, *78*, 132511.
(17) Singh, Y.; Green, M. A.; Huang, Q.; Kreyssig, A.; McQueeney, R. J.; Johnston, D. C.; Goldman, A. I. *Phys. Rev. B* **2009**, *80*, 100403.
(18) Bronger, W.; Müller, P.; Höppner, R.; Schuster, H.-U. *Z. Anorg. Allg. Chem.* **1986**, *539*, 175−182.
(19) Müller, R.; Kuckel, M.; Schuster, H.-U.; Müller, P.; Bronger, W. *J. Alloys Compd.* **1991**, *176*, 167−172.
(20) Dascoulidou, A.; Müller, P.; Bronger, W. *Z. Anorg. Allg. Chem.* **1998**, *624*, 124−128.
(21) Guo, Y. F.; Princep, A. J.; Zhang, X.; Manuel, P.; Khalyavin, D.; Mazin, I. I.; Shi, Y. G.; Boothroyd, A. T. *Phys. Rev. B* **2014**, *90*, 075120.
(22) Brock, S. L.; Raju, N. P.; Greedan, J. E.; Kauzlarich, S. M. *J. Alloys Compd.* **1996**, *237*, 9−19.
(23) Marcinkova, A.; Hansen, T. C.; Curfs, C.; Margadonna, S.; Bos, J. W. G. *Phys. Rev. B* **2010**, *82*, 174438.
(24) Emery, N.; Wildman, E. J.; Skakle, J. M. S.; McLaughlin, A. C.; Smith, R. I.; Fitch, A. N. *Phys. Rev. B* **2011**, *83*, 144429.

(25) Welter, R.; Venturini, G.; Ressouche, E.; Malaman, B. *J. Alloys Compd.* **1995**, *228*, 59−74.
(26) Tsukamoto, Y.; Okamoto, Y.; Matsuhira, K.; Whangbo, M.-H.; Hiroi, Z. *J. Phys. Soc. Jpn.* **2011**, *80*, 094708.
(27) Kimber, S. A. J.; Hill, A. H.; Zhang, Y.-Z.; Jeschke, H. O.; Valentí, R.; Ritter, C.; Schellenberg, I.; Hermes, W.; Pöttgen, R.; Argyriou, D. N. *Phys. Rev. B* **2010**, *82*, 100412(R).
(28) Shirane, G. *Acta Crystallogr.* **1959**, *12*, 282−285.
(29) Lee, C.; Kan, E.; Xiang, H.; Kremer, R. K.; Lee, S.-H.; Hiroi, Z.; Whangbo, M.-H. *Inorg. Chem.* **2012**, *51*, 6890−6897.
(30) Coelho, A. A. *TOPAS Academic: General Profile and Structure Analysis Software for Powder Diffraction Data*, 4th ed.; Bruker AXS: Karlsruhe, Germany, 2012.
(31) Larson, A. C.; Von Dreele, R. B. *GSAS Suite of Programs*; Los Alamos National Laboratory: Los Alamos, NM, 2004.
(32) Toby, B. H. *J. Appl. Crystallogr.* **2001**, *34*, 210−213.
(33) Wills, A. S. *Physica B* **2000**, *276*−*278*, 680−681.